

Modelling of Debonding Failures in FRP-Strengthened Two-Way Slabs

by W.E. El Sayed, U.A. Ebead, and K.W. Neale

Synopsis: With the development of the technology of strengthening existing concrete structures using externally bonded FRP composites, a number of issues related to the structural behaviour of such structures require investigation. One of the most important issues is the interfacial behaviour between the FRP composite and the concrete as this often controls the failure mode of the strengthened member. Several studies have progressed on the development of appropriate interfacial behaviour (bond–slip) models and on understanding the debonding phenomena. This work focuses on the numerical modelling of FRP-strengthened two-way reinforced concrete slabs where the predominant mode of failure is debonding at the FRP-concrete interface. An appropriate finite element model that represents the interfacial behaviour for FRP-strengthened two-way slabs is presented. The proposed model successfully simulates the different flexural failure modes, particularly those related to the debonding of the FRP sheets. The ultimate load carrying capacity and load–deflection relationships are predicted with reasonable accuracy.

Keywords: bond-slip model; debonding; FRP composites; interfacial behaviour; two-way slabs

462 El Sayed et al.

W.E. El Sayed, M.Sc., is a Ph.D student, Department of Civil Engineering, Université de Sherbrooke, Sherbrooke, Quebec, Canada. He received his M.Sc. from Helwan University, Cairo, Egypt in 2001. His research interests include the strengthening of reinforced concrete structures using composite materials and the finite element modelling of FRP-strengthened structures.

U.A. Ebead, Ph.D., P.Eng. is an NSERC Postdoctoral Fellow, Department of Civil Engineering, Université de Sherbrooke, and Assistant Professor at Helwan University, Cairo, Egypt. He received his Ph.D. from Memorial University of Newfoundland, Canada in 2002. His research interests include the strengthening of concrete structures and the finite element analysis of concrete structures.

K.W. Neale, Ph.D., Eng. is Canada Research Chair in Advanced Engineered Material Systems, Department of Civil Engineering, Université de Sherbrooke. His research interests include the rehabilitation and strengthening of structures using composite materials, micromechanics, solid mechanics, and materials engineering.

INTRODUCTION

FRP composites are deemed very promising materials for use as external reinforcements for reinforced concrete structural elements. As a result, there has been a numerous amount of research work conducted on the use of FRP composites in strengthening reinforced concrete structures. Several studies have been conducted on the use of FRPs for the shear strengthening of concrete slabs. In some of these studies, slabs were strengthened either with unidirectional FRP sheets around the column stub^{1,2,3} or with bidirectional FRP sheets bonded over the whole slab width⁴. Another study used L-shaped FRP plates anchored to the slab⁵. In addition, FRP strengthening materials have been used for the flexural strengthening of one-way^{6,7} and two-way slabs^{8,2,7}. In other studies, the slabs were strengthened with equally spaced FRP sheets in both directions over the whole slab width^{9,10}. Another investigation studied prestressed FRP sheets for the strengthening of two-way slabs¹¹. There are limited theoretical investigations on the behaviour of FRP-strengthened slabs. The present study attempts to provide theoretical insight on the efficiency of using FRP composites for such applications.

Finite element analysis is undoubtedly one of the most effective numerical methods for modelling the behaviour of reinforced concrete two-way slabs strengthened with FRP composites. Reitman and Yankelevsky¹² developed a new technique for the nonlinear analysis of reinforced concrete slabs under various loading conditions. Their technique used a nonlinear finite element analysis of a grid representing the slab based on yield-line theory. Seim et al.⁷ used a beam analogy to provide an approximate simulation of the overall response of FRP-strengthened one-way slabs. The moment-curvature relationship and a hypothetical three-stage load–displacement curve have been used. The hypothetical three-stage curve represented the uncracked response, the response before yielding of the steel, and the yielding of the steel and failure of either the concrete or the FRP composites. Other researchers used finite element packages to investigate the structural behaviour of concrete slabs, both unstrengthened¹³ and strengthened^{1,10}. In

another study, the strengthened slabs were designed as three-layered plates using a simplified laminated plate model⁹. The bottom layer represented the FRP strip, the middle layer represented the steel reinforcement, and the upper layer represented the compressive concrete. Usually, for the FRP-strengthened slabs, a full-bond was assumed between the concrete and the FRP composites.

From the available literature on the FRP strengthening of concrete slabs, it is clear that the amount of theoretical research is very limited compared to the experimental work. It is obvious that further analytical research is required. In this study, we attempt to enrich the theoretical research on the use of the FRPs as a strengthening technique for two-way slabs. This study introduces a nonlinear finite element analysis to simulate the behaviour of these applications. This analysis takes into account the material nonlinearity and also the FRP-concrete interfacial behaviour. The main advantage of the present numerical model is its ability to accurately represent the entire load–deflection behaviour, including crack development, and all possible failure modes such as debonding and the classical flexural failures.

FRP-CONCRETE INTERFACE

The interfacial bond between the concrete and the FRP composites has a significant effect on the overall performance of the strengthened members. Experimental studies showed that the overall behaviour is brittle for externally bonded FRP beams due to mechanisms such as delamination and/or peeling-off. Such a premature failure leads to an inefficient usage of the FRP materials and prevents the strengthened members from reaching their full capacities. Observations showed that there are two different debonding types that occur in experiments, both of which result in the delamination of the FRP sheets from the concrete^{14,15,16}. The first type of debonding takes place in the adhesive layer, where the interfacial shear strength is exceeded. The other type is represented by diagonal micro-cracks of the concrete at the interface. Existing studies suggest that the main failure mode for FRP-to-concrete bonded joints in direct shear tests is a concrete failure due to shear, occurring generally at a few millimetres from the adhesive layer inside the concrete^{17,18}.

Generally, there are two approaches for the simulation of the debonding of FRP-strengthened reinforced concrete structures using a nonlinear FE model. In the first approach, debonding is directly simulated by modelling the cracking and failure of concrete elements adjacent to the adhesive layer^{19,20}. To simulate the debonding behaviour using this approach, a very fine finite element mesh with element sizes being one order smaller than the thickness of the fracture layer of the concrete is used²⁰. This approach has the simplicity of the fixed angle crack model rather than using the rotating angle crack model and has the capability of tracing the paths of the cracks as deformation progresses. This approach is referred to as meso-scale modelling. The second approach is to use interface elements between the FRP composites and the concrete where the failure of these elements represents debonding^{21,15}. In this approach an appropriate bond–slip model needs to be employed for the interface elements. Unfortunately, the meso-scale model is difficult to be implemented in the case of three-dimensional modelling due to

the large computational demands. Thus, in this study, interface elements are used to represent the interfacial behaviour between the concrete and the FRP composites.

NONLINEAR FINITE ELEMENT MODEL

The finite element package ADINA²² is used to simulate the structural behaviour of FRP-strengthened reinforced concrete two-way slabs. This analysis considers the complexities of the interfacial behaviour, concrete nonlinearity, and the different failure modes for the concrete. A three-dimensional model is developed. A comparison between the theoretical results and the available experimental data is discussed.

MATERIAL MODELLING

Plain Concrete

A plasticity-based model is used to represent the concrete in compression and adopts the smeared crack approach for the tensile behaviour of the cracked concrete²². The stress–strain relationship of the concrete in compression exhibits a nearly linear elastic response up to about 30% of the concrete compressive strength. This is followed by a plastic behaviour until the concrete compressive strength is reached. Beyond the compressive strength, the concrete stress–strain relationship exhibits strain softening until crushing. Figure 1-a shows the idealized uniaxial stress–strain curve for the concrete, and Figure 1-b shows the biaxial failure surface of the concrete.

The stress–strain relationship for the concrete in tension is assumed to follow a linear ascending branch with a slope that is equal to the concrete modulus of elasticity, E_c , until the maximum tensile stress, σ_t , is reached as shown in Figure 1-a. In this study the smeared crack model is used, in which it is assumed that a plane of failure is developed perpendicular to the corresponding principal stress direction. The normal and shear stiffness across the plane of failure are reduced and plane stress conditions are assumed to exist at the plane of tensile failure²².

Steel Reinforcement and FRP Composites

Typical stress–strain relationships for reinforcing steel bars used in concrete are obtained from tests. For all practical purposes, steel exhibits the same stress–strain relationship in compression as in tension. This relationship can appropriately be represented by using an elastic-plastic constitutive model as shown in Figure 2-a. For the FRP composite, a linear elastic material behaviour up to failure is assumed as shown in Figure 2-b.

Bond–Slip Model

The mechanical behaviour of the FRP-concrete interface can be modelled as a relationship between the local shear stress, τ , and the relative displacement, S , between the FRP sheet and the concrete substrate. A nonlinear bond–slip model is employed in the present study²⁰. This model is a nonlinear relationship between the shear stress, τ , and the relative slip, S , as shown in Figure 3. The area under the τ – S curve presents the interfacial

fracture energy, G_f , which is defined as the energy required for complete debonding per unit bond area. The τ - S relationship is as follows:

$$\tau = \tau_{\max} \left[\sqrt{\left(\frac{S}{S_o - S_e} + \left\{ \frac{S_e}{2(S_o - S_e)} \right\}^2 \right)} - \frac{S_e}{2(S_o - S_e)} \right] \quad \text{if } S \leq S_o \quad (1)$$

$$\tau = \tau_{\max} \cdot \exp \left[\left(\frac{\tau_{\max} S_o}{G_f - G_f^a} \right) \left(1 - \frac{S}{S_o} \right) \right] \quad \text{if } S > S_o \quad (2)$$

The maximum bond strength, τ_{\max} , is governed by the tensile strength of the concrete, f_t , and the width ratio, β_w , as follows:

$$\tau_{\max} = 1.5 \beta_w f_t \quad (3)$$

where the width ratio, β_w , depends on the FRP plate width, b_f , and the concrete member width, b_c , as follows:

$$\beta_w = \sqrt{\frac{2.25 - b_f / b_c}{1.25 + b_f / b_c}} \quad (4)$$

S_o is the slip corresponding to the maximum bond strength, τ_{\max} , as shown in Figure 3. S_o has an elastic and plastic component, S_e and S_p , respectively as follows:

$$S_o = S_e + S_p = \frac{\tau_{\max}}{K_o} + 0.0195 \beta_w f_t, \quad (5)$$

K_o is the equivalent initial stiffness which depends on the elastic shear stiffness of the concrete, K_c , and that of the adhesive, K_a , as follows:

$$K_o = \frac{K_a K_c}{K_a + K_c}, \quad (6)$$

$$K_c = \frac{G_c}{t_c}, \quad K_a = \frac{G_a}{t_a}, \quad (7)$$

Here G_c and G_a are the shear moduli for the concrete and the adhesive, respectively, t_a is the thickness of the adhesive layer, and t_c is the effective thickness of the interfacial concrete layer. The thickness of this layer depends strongly on the concrete fracture energy and can be assumed to be 5 mm²³. The total fracture energy, G_f , can be expressed as:

$$G_f = 0.308 \beta_w^2 \sqrt{f_t}, \quad (8)$$

while the fracture energy of the ascending branch G_f^a , can be expressed as:

$$G_f^a = \tau_{\max} S_o \left[\frac{2A}{3} \left(\frac{1 + B^2 A}{A} \right)^{3/2} - B - \frac{2}{3} B^3 A \right] \quad (9)$$

$$\text{where } A = \frac{(S - S_o)}{S_o}, \quad B = \frac{S_e}{2(S_o - S_e)} \quad (10)$$

Due to the various applications of the bond-slip model to FRP-strengthened slabs with different configurations, it is obvious that the interfacial fracture energy is less affected by the FRP stiffness; however, it is affected by the mechanical properties of the concrete

and to a lesser extent by those of the adhesive. Further details of this model can be found in²⁰.

GEOMETRICAL MODELLING

Due to the geometrical and loading symmetry of the slabs, only one quarter of the slab was modelled. Symmetrical boundary conditions were placed along the two axes of symmetry. Figure 4 shows the configurations of the different test specimens that are investigated in this study. Figure 5 shows a FE representation of one of these specimens, tested by Ebead and Marzouk¹. For the two-way slab specimens, the strengthening materials were attached to the tension side of the slab in both directions. The orthotropy of each FRP strip was accounted for in the constitutive material properties of the corresponding elements depending on the fibre orientation. In the proposed model, in order to represent the interface elements, two sets of nodes were employed. One set of nodes was used for the concrete elements, while the second set of nodes was used for the FRP elements. These two sets of nodes were connected together using the interface elements that allow relative horizontal displacements (slip) to take place between the FRP composites and the concrete surface.

3-D quadrilateral solid elements were used to represent the concrete. Using such elements satisfies the shear and bending deformations due to their quadratic interpolation functions. The element employed has 27 nodes; each node has three degrees of freedom.

Thin shell elements were used to represent both the unidirectional and bidirectional FRP composites. The thin shell element has nine nodes; each node has three degrees of freedom.

Nonlinear translational spring elements were employed to represent the FRP-concrete interface. Each element has two nodes; each node has three degrees of freedom. These elements were employed in the same direction as that of the unidirectional fibres and in both directions for the bidirectional fibres. A force–displacement relationship was developed based on the bond–slip model used. The interface elements have only stiffness in the horizontal direction. Constraint equations were applied in the vertical direction between the concrete elements and the FRP elements.

Steel reinforcement elements embedded in the concrete are best described as one-dimensional elements. Truss elements are very appropriate to represent the steel reinforcement. Two-node truss elements were generated and connected to the 27-node 3-D solid elements. The truss element has two nodes; each node has three translational degrees of freedom. The assemblage of the various elements is shown in Figure 5.

NUMERICAL RESULTS

In order to calibrate the proposed model, a comparison was first made between the theoretical and the experimental results for one-way reinforced concrete slabs

strengthened with FRP composites. Tables 1 and 2 show the material properties for the different specimens and the different configurations are described in Table 3 and Figure 4. The comparisons are made in terms of the ultimate load carrying capacity and the load–deflection relationship. In addition, the slip profiles along the FRP plate are given.

Ultimate Load Carrying Capacity

The proposed model proved its ability to predict the ultimate load carrying capacity of the FRP-strengthened slabs with a good accuracy. Table 4 shows the comparison between the experimental and the theoretical results for the different sets of specimens. The model is able to predict the load capacity of one-way slabs as well as that for the two-way slabs. Besides, the model can predict the load capacity of both flexural and shear strengthened slabs with an accuracy of about 90%. In addition, the proposed model can successfully simulate the structural behaviour of the post-strengthened slabs including the load sequences and the application of the strengthening materials. For all the cases, FRP debonding was the common failure mode.

Load–Deflection Relationships

Comparisons between experimental and numerical results in terms of the load–deflection relationships are important to evaluate the accuracy of the model in predicting the overall behaviour and stiffness characteristics of the slabs. Figures 6 and 7 show the predicted load–deflection relationships along with the experimental results of Seim et al.⁷ and Mosallam and Mosalam¹⁰, respectively.

For the specimens of Seim et al.⁷, the load–deflection relationship follows the yield plateau of the unstrengthened slab in the case where a small amount of FRP strengthening material is employed. This was obtained for Specimen S43 that has the shortest strengthening plate length of 1090 mm. For Specimens S57.5 and S72 that have plate lengths of 1460 and 1830 mm, respectively, the load–deflection relationship stopped abruptly as shown in Figure 6. The maximum deflection value of Specimen S43 was about 20% higher than those of Specimens S57.5 and S72. The same yield plateau was obtained for Specimen SA10 of Harajli and Soudki². This specimen has the smallest width of bonded FRP of 100 mm as described in Table 3. For Specimens SA20 and SA30 (that have the strengthening plate widths of 200 and 300 mm, respectively), the load–deflection relationship stopped abruptly at about 65% of the maximum deflection of the corresponding control specimen. In addition, it was found that there is no significant difference in the response between Specimens SA20 and SA30. The maximum deflection value of Specimen SA10 was about 30% higher than those of Specimens SA20 and SA30. Based on the aforementioned discussion, it is evident that using a small amount of FRP material does not significantly affect the ductile behaviour of the strengthened slabs. By using a larger amount of FRP, the overall behaviour changes to a more brittle behaviour. Furthermore, as the strengthening plate length increases, the specimen strength increases. However, there is an optimum width of the strengthening plate beyond which no significant improvement is achieved. This agrees with other observations⁸.

Figure 7 shows the load–deflection relationships for the specimens tested by Mosallam and Mosalam¹⁰. It shows the comparison between the experimental and

theoretical results for the unreinforced and the reinforced specimens before and after strengthening. These specimens were subjected to a uniform load using a high-pressure water bag underneath the specimen. The effect of the strengthening is obvious in the stiffer behaviour observed for the strengthened specimens. Specimen Ret-85 was loaded up to 85% of the ultimate load of the control specimen. Then the strengthening materials were applied before the load continued up to failure. This was successfully simulated in the FE model by activating the FRP material at the specified load level. A good agreement was obtained with the experimental results, as shown in Figure 7-c.

Slip Profiles along the FRP-Concrete Interface

Based on the good agreement between the numerical and the experimental results using the proposed model in terms of the load capacity and deformational characteristics, some other quantities can be predicted that are difficult to measure in the laboratory. These quantities include the slip distribution along the FRP-concrete interface that will help understanding the interfacial behaviour between the FRP composites and the concrete.

Figure 8 shows the slip profiles along the FRP-concrete interface at different load levels for Specimen S43 of Seim et al.⁷. The slip profiles indicated that the main failure mode was characterized as debonding of the FRP plate; this is in agreement with the experimental observations. For Specimen S43, which has the shortest strengthening length, the final slip values at the plate end were 30% higher than those at the central zone of the slab. This explains the end plate debonding failure mode that was observed experimentally. On the other hand, the slip distribution for Specimens S57.5 and S73 is almost uniform at the final load stages as a result of the longer length of the attached FRP plate. It can be concluded that a bonded length of at least 65% of the specimen length is necessary to prevent the end plate debonding failure mode.

The specimens tested by Harajli and Soudki² experienced punching shear failure associated with a debonding of the FRP plates. It was found that increasing the FRP plate width resulted in a reduction in the slip values. This is because the wider the width of the FRP plate the more uniform the transferred shear stresses between the FRP plate and the concrete substrate, which in turn leads to a less interfacial slip. Figure 9 shows the slip profiles over the FRP plate length of Specimen SA30, which has the largest plate width of 300 mm. The slip profile shows that the slip values at the centre of the slab were significantly higher than those at the plate end at all load levels. This indicates that the delamination started at the centre of the slab then propagated towards the plate end.

The specimens tested by Mosallam and Mosalam¹⁰ were strengthened using equally-spaced FRP plates in both directions, as indicated in Table 3. The slip profiles had the same shape for the reinforced specimen, R-Str, and the unreinforced specimen, Un-Str. For the unreinforced Specimen, Un-Str, the slip values were 60% smaller than those of the reinforced specimen, R-Str. Furthermore, due to the intersection of the FRP plates in the two directions, the slip values were 50% lower at the overlapping zone than those at the adjacent zone on the curve shown in Figure 10. This means that the transverse strengthening plate contributes strongly to reducing the interfacial slip.

The numerical results for the specimens of Ebead and Marzouk¹ showed a rapid increase in the interfacial slip at the centre of the slab followed by an almost uniform distribution along the plate length until the plate end. This means that the debonding occurred under the applied load then propagated towards the plate end. Figure 11 shows the slip profiles for Specimen SGF-0.35. It was found that increasing the FRP plate stiffness leads to less interfacial slip between the FRP and the concrete. Also, the steel reinforcement ratio has no effect on the interfacial slip between the FRP and the concrete. Moreover, by comparing Figures 9 and 11, unlike Specimen SA30 of Harajli and Soudki², the slip values for Specimen SGF-0.35 of Ebead and Marzouk¹ were relatively high because this specimen failed mainly in flexure. On the other hand, the specimen of Harajli and Soudki had small slip values because it failed mainly due to punching shear.

Failure Characteristics

Debonding failure starts to occur when the slip value, S_o , that corresponds to the maximum shear stress defined in the bond slip model is reached at any point. The failure starts around the point of load application and moves towards the plate end. When there is a sufficient bond length, the failure occurs in the zone around the load point such as in the case of Specimen SGF-0.35 as indicated in Figure 11. In this figure, it is obvious that the slip values at failure are maximum 2.5 mm next to the load point. On the other hand for Specimen S43 where there is insufficient bond length, the debonding occurs at the plate ends as Figure 8 indicates from the slip distribution along the bonded length. From the slip profiles, it can be concluded that the load at which the slip values reach S_o , where the debonding starts to occur, is 15% higher than that at which intermediate flexural cracks appear. This means that debonding usually occurs due to intermediate flexural cracks (except for Specimen SA30 that failed in shear).

CONCLUSION

The use of appropriate interface elements in the FE analysis enabled very good simulations of the interfacial behaviour between the FRP and the concrete in FRP-strengthened two-way slabs. The proposed model can capture the debonding phenomena and predict the possible failure modes associated with the delamination of the FRP composites off the concrete. Also, this model has the capability to predict the slip profiles along the FRP-concrete interface. The slip profiles are useful for a better understanding of the expected debonding behaviour. By increasing the FRP plate width, more uniform stresses are transferred between the FRP plate and the concrete substrate. This results in lower slip values at the FRP-concrete interface.

ACKNOWLEDGEMENTS

This research was funded by the Natural Sciences and Engineering Research Council of Canada (NSERC) and the Canadian Network of Centres of Excellence on Intelligent Sensing for Innovative Structures (ISIS Canada). KWN is Canada Research Chair in Advanced Engineered Material Systems and the support of this program is gratefully acknowledged.

REFERENCES

1. Ebead, U.A. and Marzouk, H. (2004): Fiber-Reinforced Polymer Strengthening of Two-Way Slabs. *ACI Structural Journal*, **101**(5), 650-659.
2. Harajli, M.H. and Soudki, K.A. (2003): Shear Strengthening of Interior Slab-Column Connections Using Carbon Fibre-Reinforced Polymer Sheets. *Journal of Composites for Construction*, *ASCE*, **7**(2), 145-153.
3. Sharaf, M.H. and Soudki, K.A. (2004): Strengthening of Slab-Column Connections With Externally Bonded CFRP Strips. *Advanced Composite Materials in Bridges and Structures*, *ACMBS IV*, M. El-Badry and L. Dunasazegi, Eds., Canadian Society for Civil Engineering, 8 p.
4. Rochdi, E.H., Bigaud, D., Ferrier, E. and Hamelin, P. (2004): Strengthening of Slab-Column Connections With Externally Bonded CFRP Strips. *Advanced Composite Materials in Bridges and Structures*, *ACMBS IV*, M. El-Badry and L. Dunasazegi, Eds., Canadian Society for Civil Engineering, 8 p.
5. Biddah, A. (2004): Punching Shear Strengthening of Reinforced Concrete Slabs Using CFRP L-Shaped Plates. *Advanced Composite Materials in Bridges and Structures*, *ACMBS IV*, M. El-Badry and L. Dunasazegi, Eds., Canadian Society for Civil Engineering, 8 p.
6. Erki, M.A. and Heffernan, P.J. (1995): Reinforced Concrete Slabs Externally Strengthened With Fibre-Reinforced Plastic Materials. Proceedings of the Second International RILEM Symposium *FRPRCS-2*, L. Taerwe, Ed., University of Ghent, Belgium, 509-516.
7. Seim, W., Horman, M., Karbhari, V. and Seible, F. (2003): External FRP Post-Strengthening of Scaled Concrete Slabs. *Journal of Composites for Construction*, *ASCE*, **5**(2), 67-75.
8. Ebead, U.A. (2002): Strengthening of Reinforced Concrete Two-Way Slabs. *Ph.D. Thesis*. Memorial University of Newfoundland. St. John's, NF, Canada.
9. Limam, O., Foret, G. and Ehlrlacher, A. (2003): Reinforced Concrete Two-way Slabs Strengthened with CFRP Strips: Experimental Study and a Limit Analysis Approach. *Journal of Composite Structures*, **60**, 467-471.
10. Mosallam, A.S. and Mosalam, K.M. (2003): Strengthening of Two-Way Concrete Slabs With FRP Composite Laminates. *Construction and Building Materials*, **17**, 43-54.
11. Longworth, J., Bizindavyi, L., Wight, R.G. and Erki, A. (2004): Prestressed CFRP Sheets for Strengthening Two-Way Slabs in Flexure. *Advanced Composite Materials in Bridges and Structures*, *ACMBS IV*, M. El-Badry and L. Dunasazegi, Eds., Canadian Society for Civil Engineering, 8 p.
12. Reitman, M.A. and Yankelevsky, D.Z. (1997): A New Simplified Method for Nonlinear Reinforced Concrete Slabs Analysis. *ACI Structural Journal*, **94**(4), 399-408.

13. Marzouk, H. and Chen, Z.W. (1993): Nonlinear Analysis of Normal and High-Strength Concrete Slabs. *Canadian Journal of Civil Engineering*, **20**, 696-707.
14. Nguyen, D., Chan, T. and Cheong, H. (2001): Brittle Failure and Bond Development Length of CFRP-Concrete Beams. *Journal of Composites for Construction, ASCE*, **5**(1), 12-17.
15. Wu, Z.S. and Yin, J. (2003): Fracturing Behaviour of FRP-Strengthened Concrete Structures. *Journal of Engineering Fracture Mechanics*, **70**, 1339-1355.
16. Thomsen, H., Spacone, E., Limkatanyu, S. and Camata, G. (2004): Failure Mode Analyses of Reinforced Concrete Beams Strengthened in Flexure with Externally Bonded Fibre-Reinforced Polymers. *Journal of Composites for Construction ASCE*, **8**(2), 123-131.
17. Bizindavyi, L. and Neale, K.W. (1999): Transfer Lengths and Bond Strengths for Composites Bonded to Concrete. *Journal of Composites for Construction, ASCE*, **3**(4), 153-160.
18. Chen, J.F. and Teng, J.G. (2001): Anchorage Strength Models for FRP and Steel Plates Bonded to Concrete. *Journal of Structural Engineering, ASCE*. **127**(7): 784-791.
19. Wu, Z.S. (2003): Element-Level Study on Stress Transfer Based on Local Bond Properties. *Technical Report of JCI Technical Committee on Retrofit Technology*, 44-56.
20. Lu, X.Z., Teng, J.G., Ye, L.P. and Jiang, J.J. (2004): Bond-Slip Models for FRP Sheet/Plate-to-Concrete Interfaces. *Proceeding of 2nd International Conference of Advanced Polymer Composites for Structural Applications in Construction (ACIC)*, 10 p.
21. Wong, R.S.Y. and Vecchio, F.J. (2003): Towards Modeling of Reinforced Concrete Members With Externally Bonded Fiber-Reinforced Polymer Composite. *ACI Structural Journal*. **100**(1), 47-55.
22. ADINA (2003): Theory Manual, Version 8.1. *ADINA R & D, Inc. Watertown, USA*.
23. Lu, X.Z., Jiang, J.J., Teng, J.G. and Ye, L.P. (2004): Finite Element Models for FRP-to-Concrete Bonded Joints. *Construction and Building Materials*, (accepted for publication).

Table 1 — Concrete and steel reinforcement properties

Specimen	Concrete		Steel	
	f_c (MPa)	E_c (GPa)	f_y (MPa)	f_u (MPa)
Seim et al. ⁷	33.2	30	462	765
Harajli & Soudki ²	34.5	26.4	487	745
Mosallam and Mosalam ¹⁰	31.9	25.2	401.4	720
Ebead & Marzouk ¹	33.8	26.1	450	660

Table 2 — FRP composite and adhesive properties

Specimen	FRP type	FRP			Adhesive	
		f_t (MPa)	ϵ_u %	E (GPa)	f_t (MPa)	E (GPa)
Seim et al. ⁷	CFRP	2270	1.2	198	24.8	2.69
Harajli & Soudki ²	CFRP	3500	1.5	230	25	3.2
Mosallam & Mosalam ¹⁰	CFRP	1209	1.2	101	22.2	2.65
Ebead & Marzouk ¹	CFRP	2800	1.7	170	24.8	4.5
	GFRP	600	2.2	26.1	72.4	3.1

Table 3 — Configurations of the analyzed specimens

Set	Specimen	Configuration	FRP dimensions (mm)		
			length	width	thick.
Seim et al. ⁷	S43	43" FRP plate length	1090	50	1.19
	S57.5	57.5" FRP plate length	1460		
	S72	72" FRP plate length	1830		
Harajli & Soudki ²	SA10	100 mm FRP plate width	670	100	1.0
	SA20	200 mm FRP plate width		200	
	SA30	300 mm FRP plate width		300	
Mosallam & Mosalam ¹⁰	Un-Str	Unreinforced-Strengthened	2640	420	1.74
	R-Str	Reinforced-Strengthened	2640	420	1.74
	Ret-85	Repaired after 85% of P_u			
Ebead & Marzouk ¹	SGF-0.35	GFRP plate, $\rho = 0.35$ %	1900	300	1.0
	SCF-0.35	CFRP plate, $\rho = 0.35$ %			1.2
	SGF-0.5	GFRP plate, $\rho = 0.50$ %	1900	300	1.0
	SCF-0.5	CFRP plate, $\rho = 0.50$ %			1.2

Table 4 — Comparison between the analytical and the experimental results

Set	Specimen	Experimental		Theoretical		$\frac{P_{exp}}{P_{theo}}$
		Max. Defl. (mm)	Ultimate Load (kN)	Max. Defl. (mm)	Ultimate Load (kN)	
Seim et al. ⁷	Cont.	211.80	21.75	190.70	25.75	0.84
	S43	42.16	32.40	38.86	33.80	0.95
	S57.5	31.50	40.0	38.10	37.81	1.05
	S72	28.19	41.2	33.78	48.40	0.85
Soudki & Harajli ²	Cont	26	49	25	46	1.06
	SA10	17.5	47	21.2	46.3	1.02
	SA20	13.5	64	16.0	66.0	0.96
Mosallam & Mosalam ¹⁰	SA30	12	64	14.9	68.8	0.93
	Un-Cont	19.55	8.14	22.1	11.25	0.72
	Un-Str	59.69	47.89	63.5	42.29	1.13
	R-Cont	74.93	31.61	86.86	30.65	1.03
Ebead & Marzouk ¹	R-Str	73.15	58.9	71.12	64.17	0.91
	Ret-85	59.69	61.78	68.58	56.03	1.10
	Ref-0.35	48.5	248.5	38.9	260	0.96
	SGF-0.35	31.47	338	30.8	313	1.08
Ebead & Marzouk ¹	SCF-0.35	22.37	360	26.8	345.8	1.04
	Ref-0.5	40.65	320.1	42.0	307.4	1.04
	SGF-0.5	26.7	414.6	26.5	369.9	1.12
	SCF-0.5	24.4	448.1	21.7	405.1	1.10

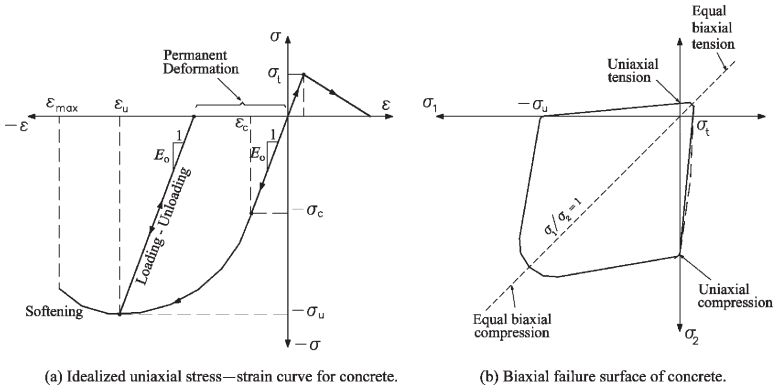


Figure 1—Constitutive model for concrete

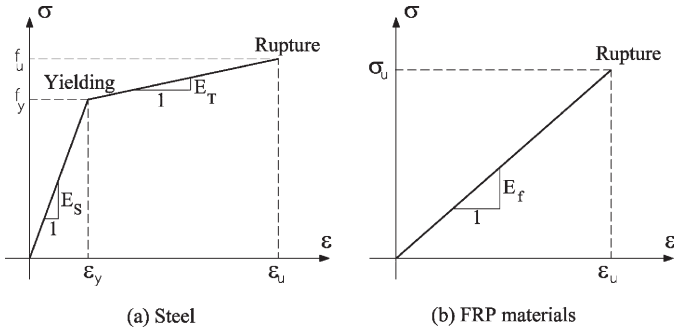


Figure 2—Typical stress-strain curves for steel and FRP materials

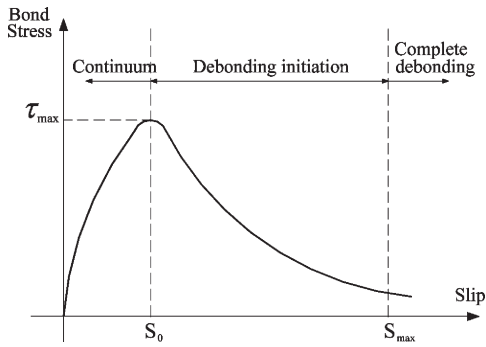


Figure 3—Bond-slip model

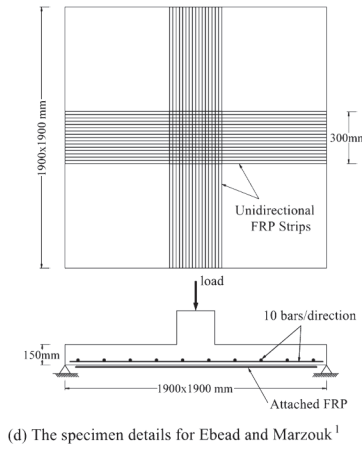
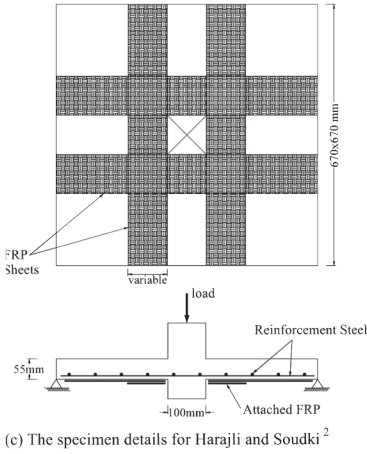
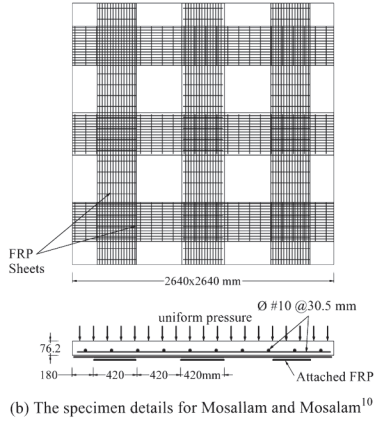
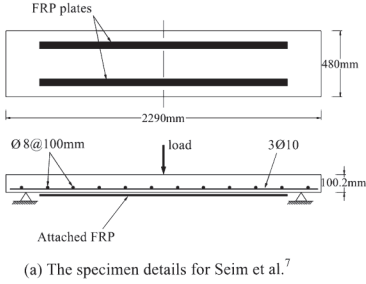


Figure 4—Configurations of the test specimens

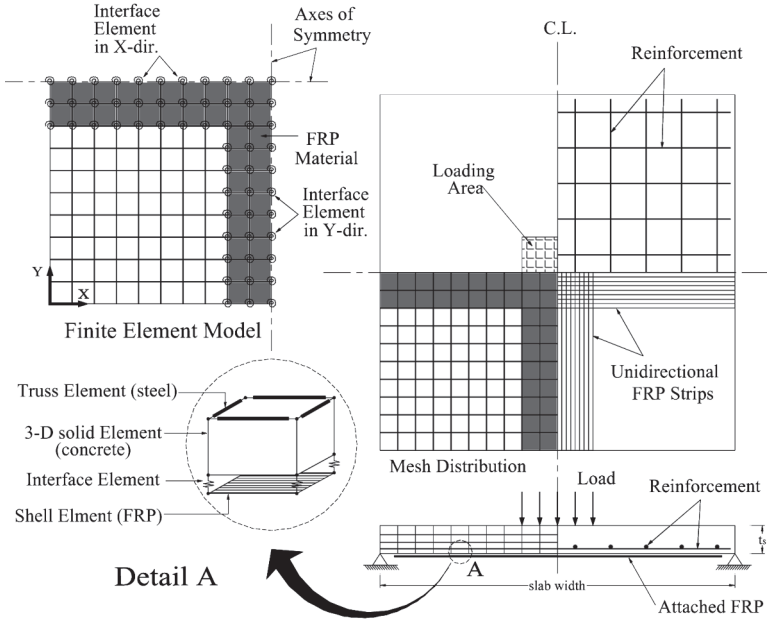


Figure 5—Typical specimen details and model description for Ebead and Marzouk¹

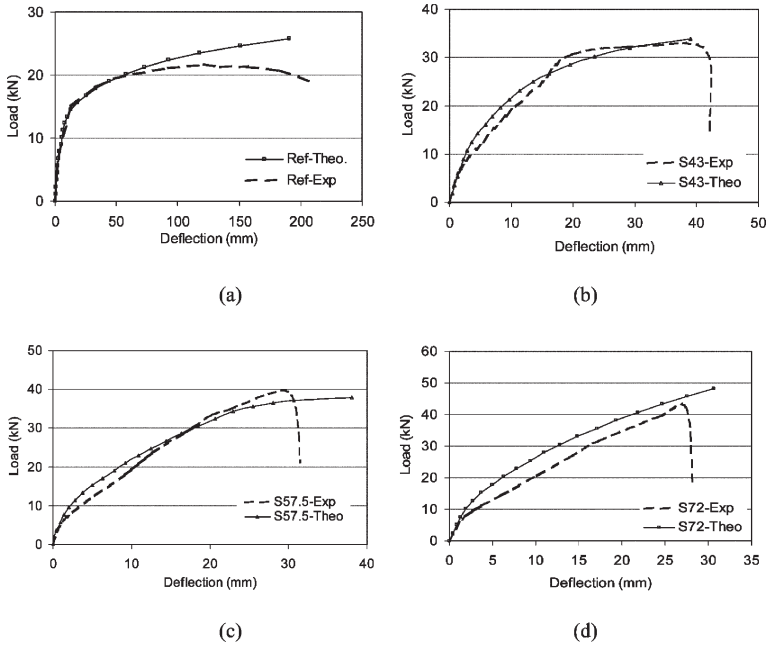
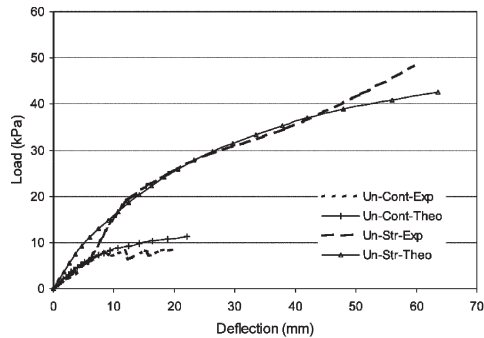
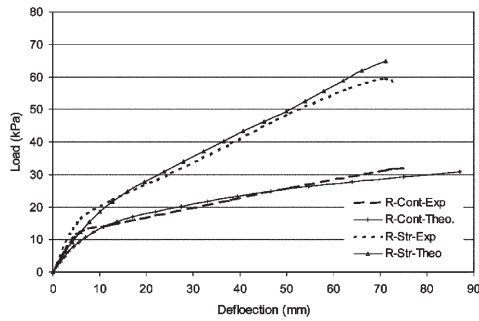


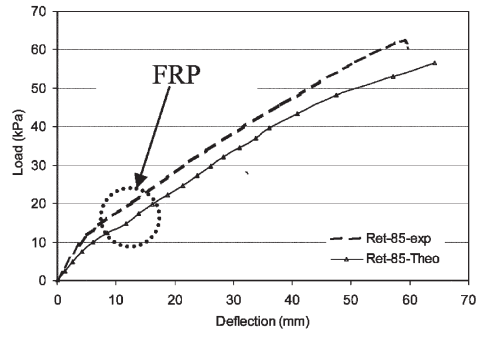
Figure 6—Comparison with test results of Seim et al. specimens⁷



(a)



(b)



(c)

Figure 7—Comparison with test results of Mosalam et al. specimens¹⁰.

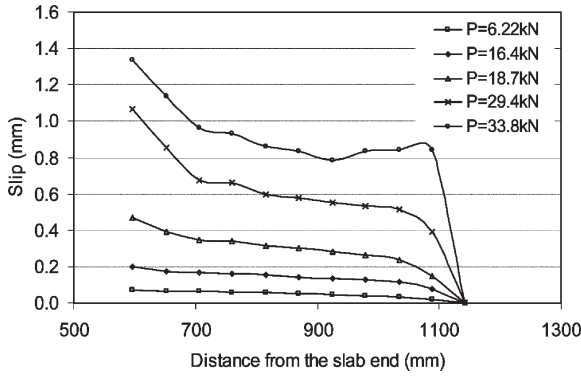


Figure 8—Slip profiles for Specimen S43 of Seim et al.⁷

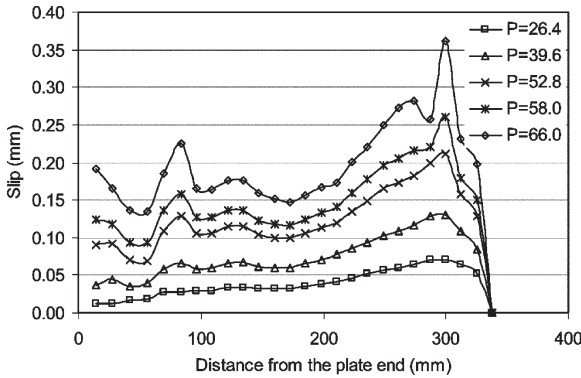


Figure 9—Slip profiles for Specimen SA30 of Harajli and Soudki²

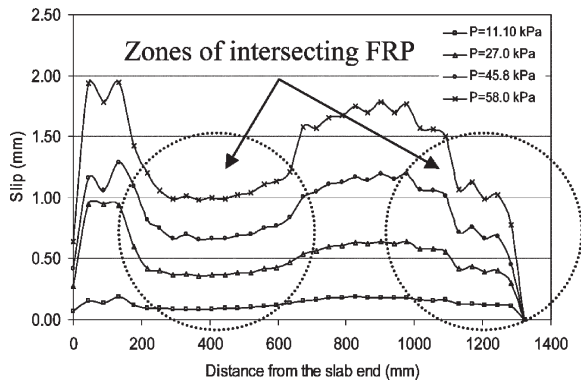


Figure 10—Slip profiles for Specimen R-Str of Mosallam and Mosalam¹⁰

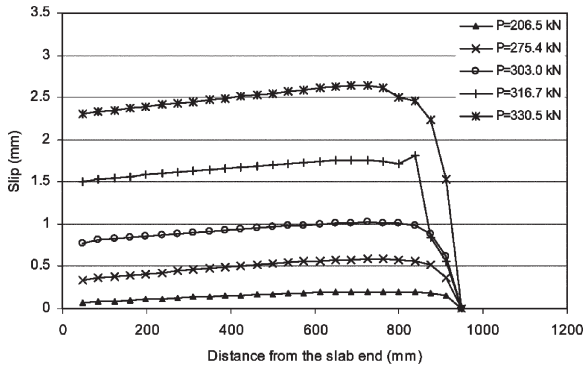


Figure 11—Slip profiles for Specimen SGF-0.35 of Ebead and Marzouk¹

